BNL-211519-2019-TECH
C-A/AP/619

Emittance growth generated by bunched beam electron cooling

M. Blaskiewicz

April 2019

Collider Accelerator Department
Brookhaven National Laboratory

U.S. Department of Energy
USDOE Office of Science (SC), High Energy Physics (HEP) (SC-25)

DISCLAIMER

Emittance Growth Generated by Bunched Beam Electron Cooling

M. Blaskiewicz, J. Kewisch
BNL 911B, Upton, NY 11973, USA

The low energy RHIC electron cooling (LEReC) project at Brookhaven employs a linac to supply electrons with kinetic energies from 1.6 to 2.6 MeV. Along with cooling the stored ion beam the electron bunches create a coherent space charge field which can cause emittance growth. This process is investigated both analytically and through simulation.

INTRODUCTION

The low energy RHIC electron cooling project is currently under construction at BNL. We are using an electron linac with bunch lengths of a few centimeters to cool gold beams with lengths of several meters. Let γ be the Lorentz factor of the ions, $\alpha_{\rm p}$ be the momentum compaction factor, $\sigma_{\rm p}$ be the rms fractional momentum spread, $\eta = 1/\gamma_t^2 - 1/\gamma^2$, and T_0 be the revolution period. The rms longitudinal slip per turn is $\sigma_{\rm slip} = T_0|\eta|\sigma_{\rm p}$. Table 1 shows this and other RHIC parameters.

TABLE I: Gold beam parameters

parameter	$\gamma = 4.1$ value	$\gamma = 6.0$ value
$\sigma_{\rm tg}$(ns)	11.7	9.6
$\sigma_{\rm p}$	3.5×10^{-4}	3.8×10^{-4}
$N_{\rm ion}$	6×10^8	1×10^9
emittance μm	2.5	2.5
f_0 (kHz)	75.8	77.2
$\sigma_{\rm slip}$(ps)	280	127

TABLE II: Electron beam parameters

parameter	$\gamma = 4.1$ value	$\gamma = 6.0$ value
$\sigma_{\rm te}$(ps)	100	67
$\sigma_{\rm p}$	$4 - 8 \times 10^{-4}$	$4 - 8 \times 10^{-4}$
$Q_{\rm e}$(pC)	$65 - 130$	78-156
emittance μm	1-2	1-2
bunch spacing (ns)	1.42	1.42
bunches per train	31	25

The electron parameters are still under discussion but ranges are shown in Table 2. In the tables $\sigma_{\rm tg}$ and $\sigma_{\rm te}$ are the root mean square (rms) bunch durations, $Q_{\rm e}$ is the electron bunch charge, and $N_{\rm ion}$ is the number of ions per bunch.The emittance is the rms normalized emittance. There is a train of electron bunches of length $\sim 4\sigma_{\rm tg}$ as illustrated in Figure 1. For all cases one has $\sigma_{\rm te} < \sigma_{\rm slip}$ which means that if an ion is subjected to a maximal space charge force on one turn it is unlikely to be subject to a significant force on the next turn. Work by Gang Wang and Vladimir Litvinenko [1] has shown that it is critical that the electron bunches not slip with respect to the ion bunches. We assume this is the case but this still leaves the possibility of synchrobetatron resonances.

To study these resonances assume the cooling section is centered on β^* with $\alpha^* = 0$ and take the transverse ion coordinates to be x and $p = \beta^* x'$ so that the one turn matrix is just a rotation with phase advance $\psi_0 = 2\pi Q_x$. As a first approximation assume a single electron bunch centered on the ion bunch so that an ion interacts with it twice per synchrotron oscillation. Assuming the electron bunch has focusing strength k an approximate map for half a synchrotron oscillation is

$$\begin{bmatrix} x_{n+1} \\ p_{n+1} \end{bmatrix} = \begin{bmatrix} \cos\frac{\pi Q_x}{Q_s} & \sin\frac{\pi Q_x}{Q_s} \\ -\sin\frac{\pi Q_x}{Q_s} & \cos\frac{\pi Q_x}{Q_s} \end{bmatrix} \begin{bmatrix} 1 & 0 \\ \beta^* k & 1 \end{bmatrix} = \begin{bmatrix} x_n \\ p_n \end{bmatrix}, \tag{1}$$

where Q_s is the synchrotron tune. When Q_x/Q_s is close to an integer the map is unstable. Taking $\sin(\pi Q_x/Q_s) = \epsilon$ and assuming an eigenvalue $\lambda = 1 + \delta$ one finds $\delta \approx \sqrt{\beta^* k\epsilon - \epsilon^2}$. The resonances for LEReC are typically very weak with $\beta^* k \sim 10^{-5}$. When coupled with the small fraction of time the ions interact with the electrons one expects a very small fraction of the beam would be harmed by these resonances. However there is another important dynamical effect. Longitudinal intrabeam scattering causes the longitudinal action to wander and with it the synchrotron tune. This causes individual particles to wander back and forth through resonances, usually increasing betatron amplitude with each passage. If we look at it in terms of statitical averages the average increase in amplitude will be proportional to the maximum growth and the fraction of time growing is proportional to the resonance width. Since both terms are linear in the charge of the electron bunch one expects the emittance growth rate to scale as the square of the electron bunch charge.

SIMULATIONS

The simulation code is based on a simple one turn map for the ions and a thin lens treatment of the electron-ion interaction. The one turn map is defined by betatron tunes, coupling, chromaticities, detuning coefficients and sine wave RF. Also we include longitudinal IBS with total growth rate given by Piwinski's [4]coasting beam formula and Zenkevich's [5] viscous force. Transverse IBS is not included because the model assumes a uniform focusing lattice which yields negative growth rates. Actual rates are about 10% of the longitudinal rates [6].Transverse space charge is implemented as a phase shift that is a function of betatron amplitude and longitudinal position within the bunch.

The electron ion interaction consists of a coherent space charge kick where the electron bunch is taken to be a three dimensional gaussian. Electron cooling is non-magnetized and treated with the Coloumb logarithm outside the integral. The local density is multiplied by a cooling force that has the same form as the electrostatic force [7]. The electron beam is assumed round and the cooling force is calculated at the start of the simulation and stored in a two dimensional array. A version where only one transverse variable is tracked has also been developed.

We begin by determining what parameters are relevant to the dynamics. Figure 2 shows results for $\gamma = 4.1$ but with 10 times the nominal electron bunch charge to speed things up. We can draw several conclusions. First, the two dimensional (2D) simulation in red with chromaticity $\xi = -2$ is quite similar to the one dimensional version shown in blue. We conclude the second transverse dimension is not fundamental to the emittance growth, justifying our earlier 1D analysis. The magenta and green curves in Figure 2 show the nihl effect of changing chromaticity. The purple and navy lines show the effect of reducing the longitudinal IBS by factors of 10 and 100, respectively. There is clearly an effect but it is weak. For no IBS the blue line shows no growth, hence some IBS is necessary for emittance growth. Finally the yellow curve shows the effect of linear RF. Clearly the growth is much reduced when the synchrotron tune does not depend on synchrotron amplitude.

Figure 3 shows the effect of 5 different initial random seeds with 1000 and 10,000 simulation particles. The slopes of all the curves are very simular showing that the emittance growth does not depend on microscopic details. Figure 4 shows the growth rate of the emittance for 2D simulations as the betatron tunes vary for 1000 and 10,000 macroparticles. The growth rates change by factors of two in a nonuniform way with tune, verifying that emittance growth is a resonant phenomena.

Figures 5 and 6 show emittance growth rates as a function of electron bunch charge for 1D and 2D beams respectively. For each curve we used linear least squares to fit

$$\ln\left[\frac{d\ln\epsilon}{dn}\right] = a + b\ln\left(Q_{\rm e}\right) + \text{error}, \tag{2}$$

with parameters a and b where $Q_{\rm e}$ is the electron bunch charge. The curves in Figures 5 and 6 are labeled by the betatron tune and the fitted value of b. For 1D we have $1.8 \le b \le 2.16$ and for 2D $1.68 \le b \le 2.14$ which agrees with the value of 2 obtained by our earlier analysis.

Figures 7 and 8 show best guess results for the situation in RHIC. For both cases the smaller emittance and lower intensity gives the best transverse cooling.

THEORY

The simulations discussed in the previous section can be explained analytically. To start we re-examine the impact of varying the IBS rates. Figure 9 shows qualitative simulations of the beam emittance for early times and Figure

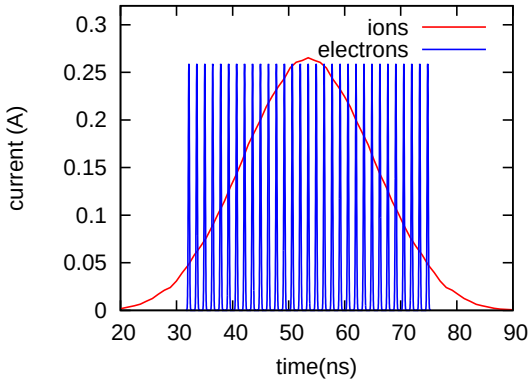

FIG. 1: Ion and electron currents for $\gamma = 4.1$ with 65 pC electron bunches.

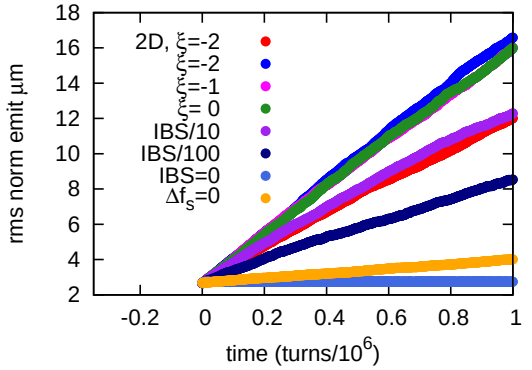

FIG. 2: Simulations of emittance growth for a range of parameters, see the text for details.

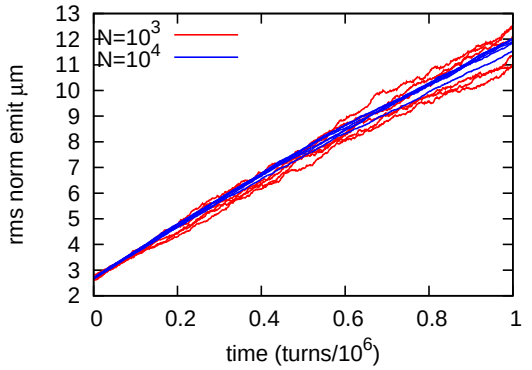

FIG. 3: Emittance versus time for identical physical parameters with different random seeds and number of simulation particles.

10 shows a more extensive simulation. For the first few thousand turns IBS rates from zero through 100 times the nominal rate all yield the same rms emittance growth. After that the emittance growth rate depends weakly on the IBS rate. It appears that the growth leads to a depletion of resonant particles and that IBS causes those particles to be replaced. From the point of view of the theory we will start by assuming that the IBS is sufficiently fast to replenish any depletion. Simulations have shown that only a single transverse dimension is needed so we consider the Hamiltonian

$$H(x,p) = \frac{Q_x}{2}\left(p^2+x^2\right) + \delta_p(\theta)a^2\Delta\psi_x(\tau)\ln\left(1+\frac{x^2}{a^2}\right), \tag{3}$$

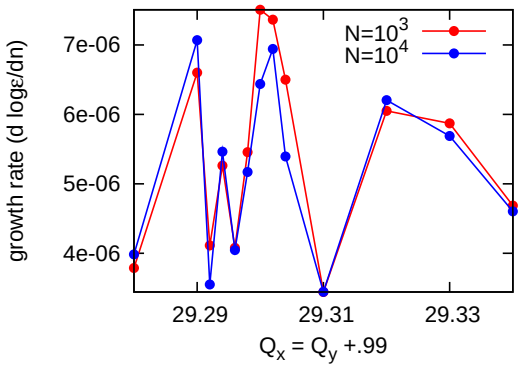

FIG. 4: Growth rate as a function of betatron tune. The fine structure implies many resonances are relevant.

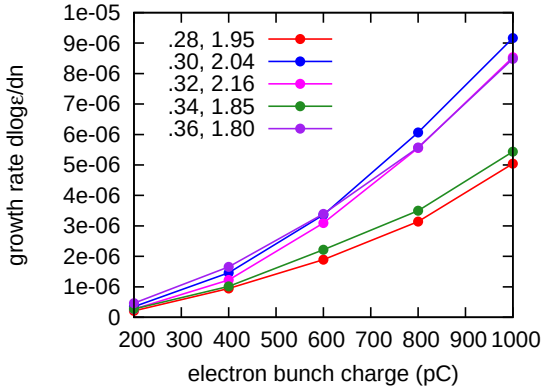

FIG. 5: Growth rate versus bunch charge for 1D simulations. The curves are labeled by the non-integer part of the betatron tune and the power law for the growth rate obtained by fitting equation (2).

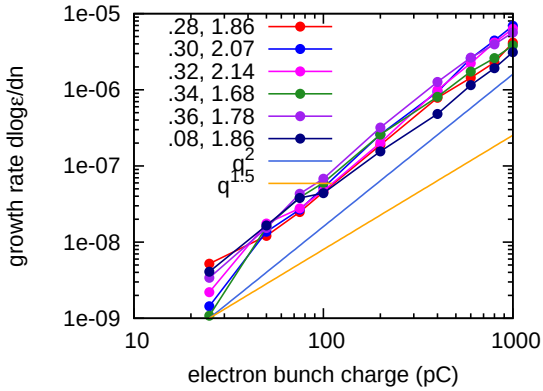

FIG. 6: Growth rate versus bunch charge for 2D simulations. The curves are labeled by the non-integer part of the betatron tune and the power law for the growth rate obtained by fitting equation (2). Curves for power laws of 1.5 and 2 are shown for comparison.

where we use azimuth θ as the time-like variable, a is the nominal radius of the electron beam, $\tau = \tau(\theta)$ is the arrival time of the ion relative to the synchronous particle, x and p are the transverse position and momentum variables, $\Delta\psi_x(\tau)$ is the space charge induced, betatron phase shift of the ions from the electrons, and

$$\delta_p(\theta) = \sum_{k=-\infty}^{\infty} \delta(\theta - 2\pi k) = \sum_{m=0}^{\infty} \frac{\cos(m\theta)}{(1+\delta_{m,0})\pi},$$

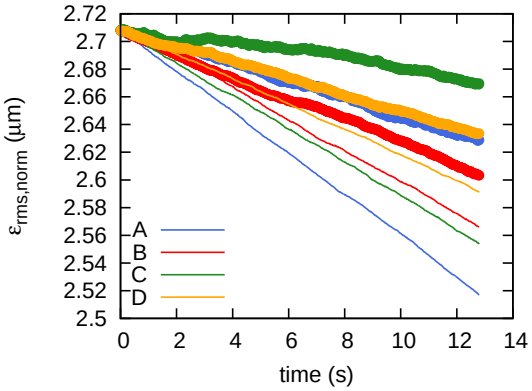

FIG. 7: Ion emittance versus time for $\gamma = 4.1$. The thick lines show the predicted behavior while the thin lines neglect the coherent kicks from the electrons. There are four cases with different rms momentum spread σ_p, rms normalized emittance ϵ and electron bunch charge Q_e. The stated electron bunch charge was used for the coherent kick while the charge used for cooling was 30% less.
A, $\sigma_\mathrm{p} = 4 \times 10^{-4}$, $\epsilon = 2$ μm, $Q_\mathrm{e} = 130$ pC;
B, $\sigma_\mathrm{p} = 4 \times 10^{-4}$, $\epsilon = 1$ μm, $Q_\mathrm{e} = 65$ pC;
C, $\sigma_\mathrm{p} = 8 \times 10^{-4}$, $\epsilon = 2$ μm, $Q_\mathrm{e} = 130$ pC;
D, $\sigma_\mathrm{p} = 8 \times 10^{-4}$, $\epsilon = 1$ μm, $Q_\mathrm{e} = 65$ pC.

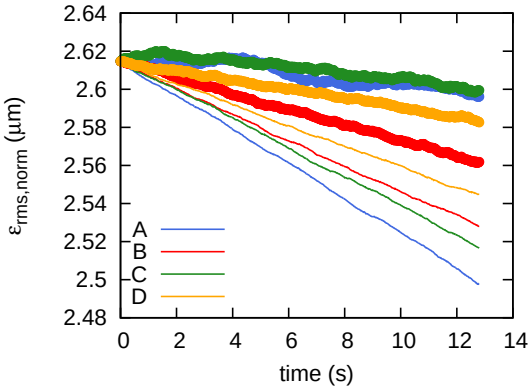

FIG. 8: Ion emittance versus time for $\gamma = 6$. The thick lines show the predicted behavior while the thin lines neglect the coherent kicks from the electrons. There are four cases with different rms momentum spread σ_p, rms normalized emittance ϵ and electron bunch charge Q_e. The stated electron bunch charge was used for the coherent kick while the charge used for cooling was 30% less.
A, $\sigma_\mathrm{p} = 4 \times 10^{-4}$, $\epsilon = 2$ μm, $Q_\mathrm{e} = 156$ pC;
B, $\sigma_\mathrm{p} = 4 \times 10^{-4}$, $\epsilon = 1$ μm, $Q_\mathrm{e} = 78$ pC;
C, $\sigma_\mathrm{p} = 8 \times 10^{-4}$, $\epsilon = 2$ μm, $Q_\mathrm{e} = 156$ pC;
D, $\sigma_\mathrm{p} = 8 \times 10^{-4}$, $\epsilon = 1$ μm, $Q_\mathrm{e} = 78$ pC.

where $\delta_{m,0}$ is the Kronecker delta. First we use action angle variables with $x = \sqrt{2J}\cos\psi$, $p = -\sqrt{2J}\sin\psi$ yielding.

$$H(\psi, J) = Q_x J + \delta_p(\theta) a^2 \Delta\psi_x(\tau) \ln\left(1 + \frac{2J\cos^2\psi}{a^2}\right) \tag{4}$$

$$= Q_x J + \delta_p(\theta)\Delta\psi_x(\tau) \sum_{n=0}^{\infty} a_n(J)\cos(2n\psi). \tag{5}$$

For $n = 0$ we find [3]

$$a_0(J) = a^2 \ln\left(\frac{1 + J/a^2 + \sqrt{1 + 2J/a^2}}{2}\right). \tag{6}$$

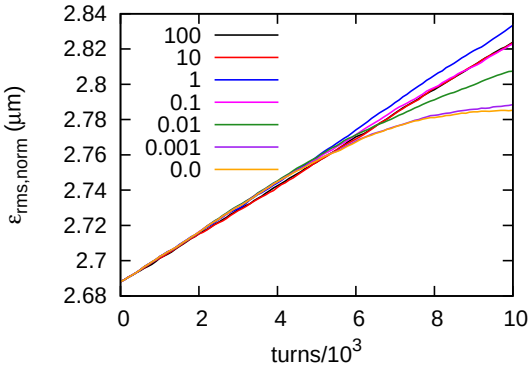

FIG. 9: Emittance growth with electron bunches of 10 times nominal charge for a range of longitudinal IBS rates. The nominal IBS growth time is 650 seconds, labeled by 1. The labels are proportional to the rates, and saturation occurs for the nominal rate and faster rates.

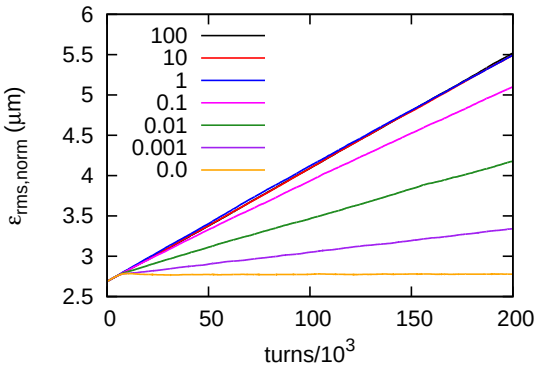

FIG. 10: Emittance growth with electron bunches of 10 times nominal charge for a range of longitudinal IBS rates. This is an extended plot of the simulations in Figure 9

For $n > 0$

$$a_n(J) = \frac{-2a^2}{n}\left(\frac{-J/a^2}{1 + J/a^2 + \sqrt{1 + 2J/a^2}}\right)^n. \tag{7}$$

The detuning term in the Hamiltonian increases without bound as J increases but the change in tune will be quite small. The other terms $a_n(J)$ are bounded by $2a^2/n$ so the driving terms saturate with betatron amplitude. We will be examining resonant behavior with small driving terms so we consider a single betatron harmonic

$$H_1(\psi, J) = Q_x J + \delta_p(\theta)\Delta\psi_x(\tau)a_n(J)\cos(2n\psi). \tag{8}$$

This Hamiltonian is straight forward to simulate but the delta function makes it difficult analytically.

To proceed take the slow approximation and make the substitution

$$\delta_p(\theta)\cos(2n\psi) \to \frac{\cos(2n\psi - p\theta)}{2\pi},$$

where, since $Q_s \ll 1$, p is chosen to minimize $|p - 2nQ_x|$. Next do a scale transformation with $\Psi = 2n\psi - p\theta$. The action variable is unchanged. The new Hamiltonian is

$$H_2(\Psi, J) = (2nQ_x - p)J + 2n\Delta Q_x C(\tau)a_n(J)\cos\Psi, \tag{9}$$

where ΔQ_x is the maximum tune shift of the ions due to the electrons and $C(\tau)$ is the ratio of electron current to peak electron current. To solve (9) we define

$$\tilde{x} = \sqrt{2J}\cos\Psi, \quad \tilde{p} = -\sqrt{2J}\sin\Psi, \quad \kappa = 2nQ_x - p.$$

Also let

$$\epsilon(J) = 2n\Delta Q_x a_n(J)/\sqrt{2J}.$$

With these definitions

$$H_2(\tilde{x},\tilde{p}) = \frac{\kappa}{2}\left(\tilde{x}^2+\tilde{p}^2\right) + \tilde{x}C(\tau)\epsilon(J). \tag{10}$$

The equations of motion are

$$\frac{d\tilde{x}}{d\theta} = \frac{\partial H_2}{\partial \tilde{p}} = \kappa\tilde{p} + \tilde{x}\tilde{p}\epsilon'(J)C(\tau) \tag{11}$$

$$\frac{d\tilde{p}}{d\theta} = -\frac{\partial H_2}{\partial \tilde{x}} = -\kappa\tilde{x} - \epsilon(J)C(\tau) - \tilde{x}^2\epsilon'(J)C(\tau). \tag{12}$$

We will solve (11) and (12) approximately. The zeroeth order approximation is to ignore the terms proportional to $\tilde{x}\tilde{p}$ and $\tilde{x}^2$, and the first order approximation is to take $\tilde{x}^2 \approx J$. Note that J will evolve slowly for weak driving terms. Define $u = \tilde{p} + i\tilde{x}$ and approximate

$$\frac{du}{d\theta} = i\kappa u - \alpha_q C(\tau), \tag{13}$$

where we allow for two approximations with $\alpha_0 = \epsilon(J_0)$ or $\alpha_1 = \epsilon(J_0) + J_0\epsilon'(J_0)$; J_0 is the initial value of J. To proceed we take $C(\tau) = -C(\tau)$ and $\tau = \hat{\tau}\sin\psi_s$ so that,

$$C(\tau) = \sum_{m=0}^{\infty} C_m(\hat{\tau})\cos(m\psi_s(\theta)), \tag{14}$$

where $\hat{\tau}$ is the synchrotron amplitude and ψ_s is the synchrotron phase. This is approximate since an arbitrary RF waveform will not yield sinusoidal oscillations, but a sine wave with an amplitude dependent tune should be an adequate approximation as long as Q_s does not get too small. It is clear that the variation in $\hat{\tau}$ leads to changes in synchrotron frequency and subsequently the synchrotron phase. However in the initial stages we want to make a detailed investigation of the parameter space. Hence we assume that $\hat{\tau}$, and subsequently C_m, remains constant and that ψ_s is a random variable. Integrating (13) one gets

$$\Delta u = u(\theta) - u_0 e^{i\kappa\theta} = -\int_0^{\theta} d\theta_1 e^{i\kappa(\theta-\theta_1)}\alpha_q \sum_{m=0}^{\infty} C_m(\hat{\tau})\cos(m\psi_s(\theta_1)), \tag{15}$$

To characterize emittance growth note that u_0 is uncorrelated with Δu and take $< |\Delta u(\theta)|^2 >$ where angular brackets denote statistical averages,

$$< |\Delta u(\theta)|^2 > = \alpha_q^2 \int_0^{\theta} d\theta_1 \int_0^{\theta} d\theta_2 e^{i\kappa(\theta_2-\theta_1)} \sum_{m,k} C_m C_k < \cos(m\psi_s(\theta_1))\cos(k\psi_s(\theta_2)) > . \tag{16}$$

Now we have

$$\psi_s(\theta) = \psi_s(0) + \int_0^{\theta} d\theta_1 Q_s(\theta_1),$$

where $\psi_s(0)$ is distributed uniformly on $[0, 2\pi)$ and $Q_s(\theta)$ is the time dependent synchrotron tune. We approximate the synchrotron tune as a stationary random variable. Averaging over $\psi_s(0)$ only the terms with $m = k$ survive. Define $\chi = \theta_2 - \theta_1$ so that

$$< |\Delta u(\theta)|^2 > = \alpha_q^2 \int_{-\theta}^{\theta} d\chi(\theta - |\chi|)e^{i\kappa\chi} \sum_{m=0}^{\infty}(1+\delta_{m,0})\frac{C_m^2}{2} < \cos[m\int_0^{\chi} Q_s(\chi_1)d\chi_1] > . \tag{17}$$

In (17) we need to evaluate the expectation value of the cosine term. The synchrotron tune varies over the IBS time which is much longer than any correlation time. Therefore the expectation value is totally dominated by fluctuations in the initial value of Q_s and is unaffected by any fluctuations in Q_s that occur on $[0, \chi]$. Additionally we will assume that Q_s is a gaussian random variable with mean $\bar{Q}_s$ and standard deviation σ_s. Then

$$< \cos[m \int_0^\chi Q_s(\chi_1) d\chi_1] >= \cos(m\bar{Q}_s\chi) e^{-m^2\sigma_s^2\chi^2/2}$$

The spread in synchrotron tune is typically $\gtrsim 1\%$ while IBS timescales are several minutes. For $m > 0$ the argument of the exponential will be very large for values of χ that are short compared to IBS timescales, verifying the previous assumption. This explains the behavior in Figure 9. For early times the emittance growth only depends on the initial variation in Q_s. After the resonant particles reach large amplitude they saturate and for the emittance to continue growing other particles must become resonant. This refreshing of the resonant reservoir is due to IBS. As long as the IBS is sufficiently fast the reservoir is always full and the growth in rms is steady.

For $\theta\sigma_s \gg 1$ and $\kappa \neq 0$, $< |\Delta u(\theta)|^2 >$ grows linearly with θ

$$\frac{d < |\Delta u(\theta)|^2 >}{d\theta} \equiv < |\Delta u(\theta)|^2 >' = \alpha_q^2 \int_{-\infty}^{\infty} d\chi \sum_{m=1}^{\infty} \frac{C_m^2}{2} \cos(m\bar{Q}_s\chi) e^{-m^2\sigma_s^2\chi^2/2 + i\kappa\chi}. \tag{18}$$

Notice that the $m = 0$ term is absent in (18). This is because we assume $\kappa \neq 0$. Otherwise the $m = 0$ term would grow as θ^2 and lead to unacceptable growth. The integrals in (18) over χ are straightforward and naturally break into two terms

$$< |\Delta u(\theta)|^2 >' = < |\Delta u(\theta)|_-^2 >' + < |\Delta u(\theta)|_+^2 >' \tag{19}$$

with

$$< |\Delta u(\theta)|_\pm^2 >' = \alpha_q^2 \sum_{m=1}^{\infty} \frac{\sqrt{2\pi} C_m^2}{4m\sigma_s} \exp\left(-\frac{1}{2} \left[\frac{m\bar{Q}_s \pm \kappa}{m\sigma_s} \right]^2 \right) \tag{20}$$

Equations (19) and (20) are the main results. To test them we will use $C(\tau) = 1/(1 + \tau^2)$. With $\tau = \hat{\tau} \sin\psi_s$ only the even terms in equation (14) are nonzero. The fourier coefficients can be found in closed form [3]

$$C_{2m}(\hat{\tau}) = \frac{2}{(1 + \hat{\tau}^2/2)\sqrt{1 - z^2}} \left(\frac{1 - \sqrt{1 - z^2}}{z} \right)^{2m}, \tag{21}$$

where $z = \hat{\tau}^2/(2 + \hat{\tau}^2)$.

COMPARISON WITH SIMULATIONS

A code was written to simulate (8). To maximize resolution all the simulation particles start with the same values of J and $\hat{\tau}$. The synchrotron motion was modeled as a random process with the tunes modeled as identical, independently distributed gaussian processes updated once per turn

$$\bar{\psi}_s = \psi_s + 2\pi[\bar{Q}_s + q] \tag{22}$$

$$\bar{q} = rq + \sigma_s\sqrt{1 - r^2}n, \tag{23}$$

where $0 \leq r \leq 1$ defines the correlation time scale, n is a zero mean unit standard deviation gaussian deviate, and the overbars denote updated values.

The update for the thin lens kick of the electrons on the ions was done using a canonical transformation of Goldstein's 3rd type [8]. The initial variables are J, ψ and the updated variables are $\bar{J}, \bar{\psi}$ with generator $F(J, \bar{\psi}) = \Delta\psi_x(\tau) a_n(J) \cos(2n\bar{\psi})$

$$\bar{\psi} = \psi + \frac{\partial F(J, \bar{\psi})}{\partial J} \tag{24}$$

$$\bar{J} = J - \frac{\partial F(J, \bar{\psi})}{\partial \bar{\psi}}. \tag{25}$$

Equation (24) was solved iteratively with

$$\bar{\psi}_{n+1} = \psi + \Delta\psi_x(\tau)a'_n(J)\cos(2n\bar{\psi}_n)$$

and $\bar{\psi}_0 = \psi$. For our purposes $n = 5$ was completely adequate. Figure 11 shows initial and final transverse coordinates of a typical simulation and Figure 12 shows the rms emittance versus turn. We go on to compare these simulations with equations (19) and (20).

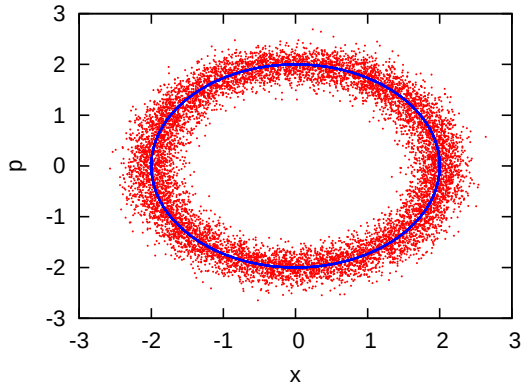

FIG. 11: Initial (blue) and final (red) particle coordinates for a simulation with 10^4 particles.

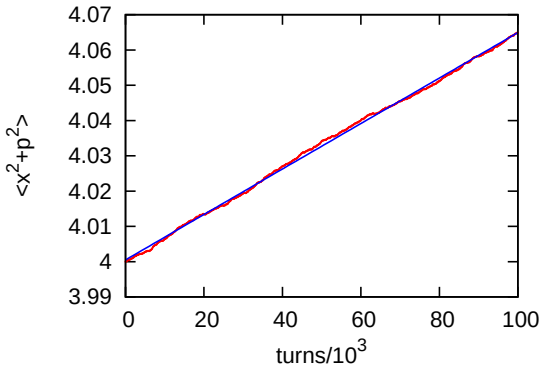

FIG. 12: $< |u|^2 >$ versus time for a simulation with 10^5 particles and the same beam parameters as in Figure 11. The simulation data are in red and the blue line is a least squares fit. The slope of the line is the emittance growth and is to be compared with equations (19) and (20).

Figure 13 Shows growth rate from simulations for betatron harmonic $n = 2$ along with the analytic estimates and a simulation using the full Hamiltonian in equation (3). The only place a significant discrepancy exists is at the extreme left for small Q_x. Here the simulation using the full Hamiltonian appears to fix on a different resonance yielding a significantly larger growth rate. Other than that the techniques are all within a factor of 2. We go on to focus on the analytic estimates and simulations using a single betatron harmonic. Figure 14 and 15 show results for betatron harmonic $n = 1$ with different values of synchrotron amplitude $\hat{\tau}$. Figure 16 shows growth as a function of $\hat{\tau}$ for $n = 2$ with other parameters fixed.For all these cases the betatron amplitude was fairly low. Figure 17 shows what can happen for betatron amplitudes large compared to the electron beam radius. In any case one can see that the formula and simulations give quantitatively comparable results so that equations (19) and (20) can be used for reliable factor of 2 estimates.

A MORE REALISTIC THEORY

The theory of the previous section is amenable to detailed comparison with simulations but it is somewhat artificial. A more physical theory can be obtained by putting C_m^2 back under the expectation value in equation (17). Once this

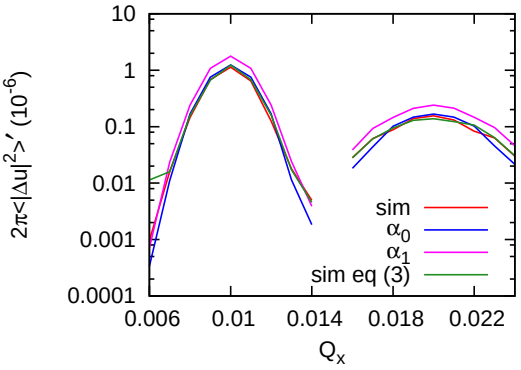

FIG. 13: Emittance growth rates for $n = 1$, $J = 2a^2$, $\hat{\tau} = 3$ as a function of betatron tune. The formulas for α_0, α_1 and a simulation using the full Hamiltonian in eq (3) are also shown.

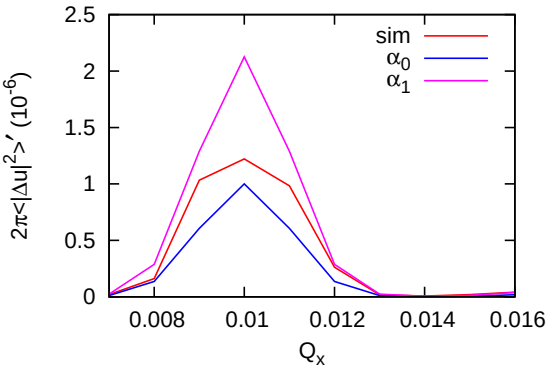

FIG. 14: Emittance growth rates for $n = 1$, $J = a^2/2$, $\hat{\tau} = 3$ as a function of betatron tune. The formula for α_0 and α_1 bracket the simulation.

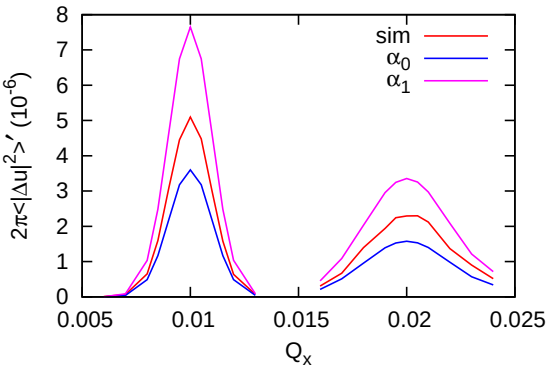

FIG. 15: Emittance growth rates for $n = 1$, $J = a^2/2$, $\hat{\tau} = 30$ as a function of betatron tune. The formula for α_0 and α_1 bracket the simulation.

is done we assume Q_s is a function soley of τ. We take the derivative of $< |\Delta u(\theta)|^2 >$ with respect to θ assuming large θ, which yields

$$< |\Delta u(\theta)|^2 >' = \frac{\alpha_q^2}{2} \int_{-\infty}^{\infty} d\chi e^{i\kappa\chi} \sum_{m=1}^{\infty} < C_m^2(\hat{\tau}) \cos[mQ_s(\hat{\tau})\chi] >_{\hat{\tau}} . \tag{26}$$

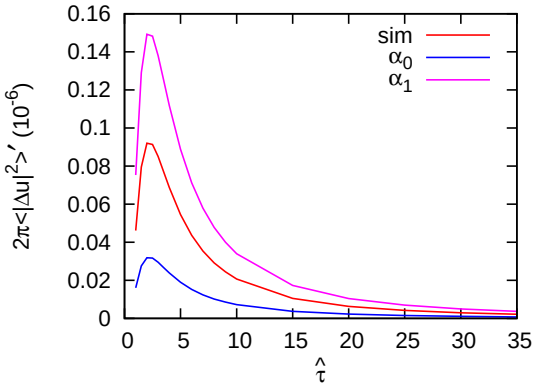

FIG. 16: Emittance growth rates for $n = 2$, $J = a^2/2$ versus $\hat{\tau}$

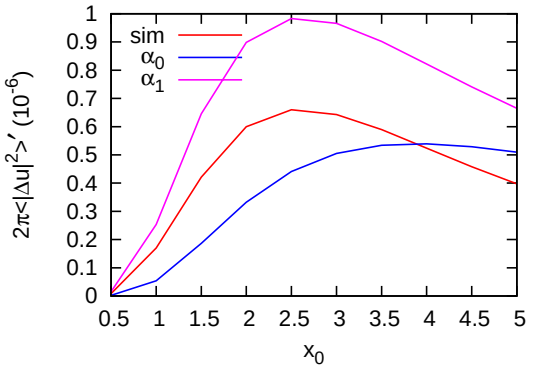

FIG. 17: Emittance growth rates for $n = 2$, $\hat{\tau} = 30$ as a function of $x_0 = \sqrt{2J}/a$. For large betatron amplitudes the formulas overestimate the growth.

In equation (26) we have assumed $\kappa \neq 0$. The averaging over $\hat{\tau}$ is accomplished by averaging over the distribution $\rho(\hat{\tau})$ with

$$\int_0^\infty \rho(\hat{\tau}) d\hat{\tau} = 1.$$

Interchanging the order of the sum and integrations yields

$$< |\Delta u(\theta)|^2 >' = \frac{\alpha_q^2}{2} \sum_{m=1}^{\infty} \int_0^\infty \rho(\hat{\tau}) C_m^2(\hat{\tau}) d\hat{\tau} \int_{-\infty}^{\infty} d\chi e^{i\kappa\chi} \cos[mQ_s(\hat{\tau})\chi]. \tag{27}$$

$$= \frac{\pi\alpha_q^2}{2} \sum_{m=1}^{\infty} \int_0^\infty \rho(\hat{\tau}) C_m^2(\hat{\tau}) \delta[|\kappa| - mQ_s(\hat{\tau})] d\hat{\tau} \tag{28}$$

$$= \frac{\pi\alpha_q^2}{2} \sum_{m=1}^{\infty} \sum_k \frac{\rho(\hat{\tau}_{k,m}) C_m^2(\hat{\tau}_{k,m})}{|mQ_s'(\hat{\tau}_{k,m})|}, \tag{29}$$

where Q_s' is the derivative of Q_s with respect to $\hat{\tau}$ and we define $\hat{\tau}_{k,m}$ to be the kth solution to $|\kappa| = mQ_s(\hat{\tau})$, where of course there may be no solutions. Equation (27) is expressed in parameters that can be unambiguously obtained from the physical parameters of the ion beam and cooling system. To test the accuracy of (29) we take C_m as defined in equation (21). We assume elliptical trajectories in the longitudinal phase space and take the synchrotron tune to

vary as

$$Q_s(J_s) = Q_0 + \frac{Q_1 J_s}{1 + (Q_2 J_s)^2} \tag{30}$$

where the Q_i are constants, $J_s = \hat{\tau}^2/2$ and $\tau(\theta) = \hat{\tau}\sin(Q_s(\hat{\tau})\theta + \psi_0)$. We take $\rho(\hat{\tau}) = \hat{\tau}\exp(-\hat{\tau}^2/2\sigma_t^2)/\sigma_t^2$ and start the simulations as before with all particles at a single value of transverse action.

Figure 18 shows the synchrotron tune and longitudinal density used. The $n = 1$ results are shown in Figure 19, along with results obtained using the full kick $\propto x/(a^2+x^2)$. The two simulation results are very similar, verifying that only a single betatron sideband is needed. Comparing the simulations with equation (29) we see that the calculation falls short by about a factor of 2. Figure 20 shows results for $n = 2$ and a similar discrepancy is seen. For both cases the growth rate obtained from the formula is about half the value seen in the simulation. Other simulations have been done and we see a similar discrepancy. To test for some sort of nonlinear behavior consider figure 21 which shows the growth rate versus ΔQ_{sc}. The growth rate scales quadratically with space charge tune shift over two orders of magnitude in space charge tune shift. The nearly perfect scaling shows that it is unlikely that higher orders in pertubation theory are important. This leaves us in the position of not being able to account for the discrepancy between the simulations and formula (29) shown in figures 19 and 20. We leave the resolution of this discrepancy to future work.

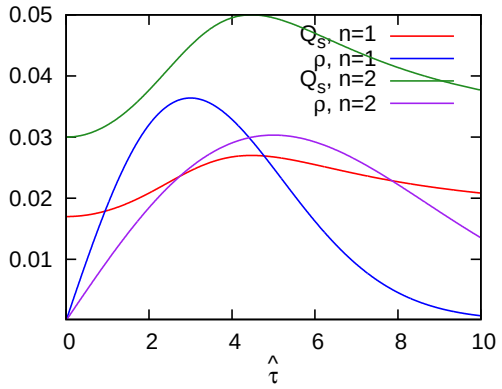

FIG. 18: Synchrotron tune and longitudinal density function versus longitudinal amplitude. The parameters for both the $n = 1$ and $n = 2$ calculations are shown.

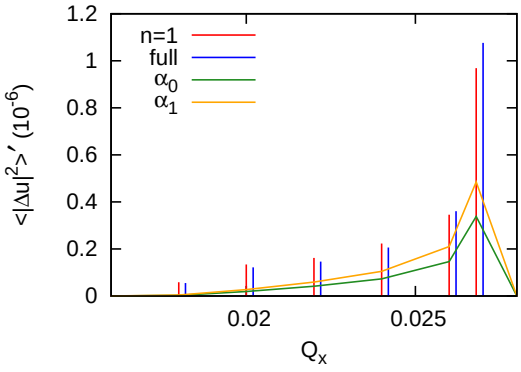

FIG. 19: Growth rates for $n = 1$ single sideband calculations along with those for the full space charge Hamiltonian. The solid lines are calculated using equation 29.

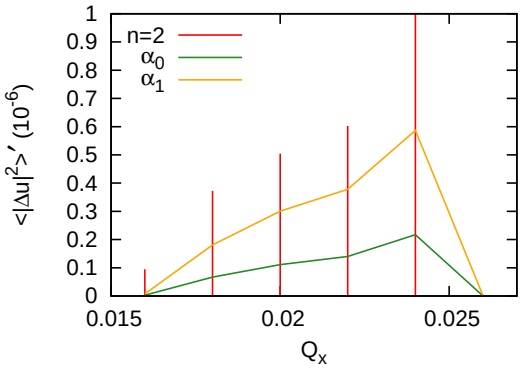

FIG. 20: Growth rates for $n = 2$ single sideband calculations. The solid lines are calculated using equation (29).

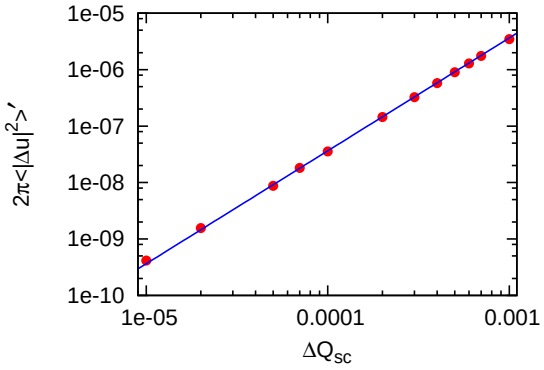

FIG. 21: Growth rate versus peak space charge tune shift. The solid line is a least squares fit assuming the growth is proportional to ΔQ_{sc}^2.

CONCLUSION

Using bunched beams for electron cooling can lead to dynamically generated emittance growth. There are 3 required ingredients:

1. electron bunches that are of comparable length to the rms longitudinal slip per turn of the ions,
2. variation of the synchrotron frequency with amplitude,
3. longitudinal intrabeam scattering, although the dependence on rates is weak.

The emittance growth rate of the ions scales like the square of the electron bunch charge. This was shown theoretically and verified using simulations. A theoretical model was developed and compared well with experiments. A more physical model was developed as well. The latter can be directly applied to a particlular accelerator and yields estimates accurate at the factor of 2 level. This should be useful in the design phase and, when showing a negligible effect, be adequate to resolve any questions.

ACKNOWLEDGMENT

This work followed from earlier work by Gang Wang and Vladimir Litvinenko. Thanks to Alexei Fedotov, Wolfram Fischer, Yun Luo, Geoffrey Krafft (of JLAB) and Christoph Montag for useful discussions. Extra thanks to Wolfram Fischer for careful reading of the manuscript.

[1] G. Wang C-A/AP/536 (2015).
[2] See e.g. section 27 of Landau and Lifshitz, *Mechanics* 3rd edition, Pergamon (1989).
[3] See 4.224.9 and 3.613.3 in Gradshteyn and Ryzhik *Table of Integrals Series and Products* academic press, 1980.
[4] A. Piwinski in *Handbook of Accelerator Physics and Engineering*, Eds A. Chao and M. Tigner, p125, World Scientific (1999)
[5] P. Zenkevich, O. Boine-Frankenheim, A. Bolshakov, NIMA, Vol 561, Issue 2, p284 (2006).
[6] Alexei Fedotov, *private communication.*
[7] H. Poth, Physics Reports, Volume 96, No 3&4 (1990).
[8] H. Goldstein, *Classical Mechanics*, Addison Wesley, (1981).